Imaging Momentum–Space Two-Particle Correlations at Surfaces

Frank O. Schumann,* Jürgen Kirschner, and Jamal Berakdar

Photoelectron and electron energy loss spectroscopies have been highly instrumental in revealing the various facets of electronic properties of materials. For a direct insight into two-particle correlations, a technique is needed that resolves two emitted electrons in coincidence. Herein, an overview on the experimental realization of correlation spectroscopy and the interpretation of the recorded spectra from theory is provided. The relation of the measured spectra to the details of the spin-, energy- and wavevector-resolved electron–electron interactions is focused upon. To disentangle the contributions of exchange from the charge-density correlation, positrons instead of electrons are used as projectiles. The short intrinsic time of the Auger decay and the neutralization of He^{2+} ions near a surface are used to estimate the characteristic timescale for the correlated electron dynamics in metals to be 40–400 attoseconds. The potential of conducting double photoemission studies with pulsed laser-based light sources is addressed.

1. General Features of Two-Particle Emission

The most detailed information on matter such as their electronic structure and the effects of coupling between various degrees of freedom is gained via photoelectron and electron-scattering spectroscopies.[1] In the widely used photoelectron emission spectroscopy for instance, an electron is released from the sample upon absorption of a single photon. From the known photon and photoelectron energies we can deduce the energetic position of the initial state whereas the energetic spread of the photoelectron peak delivers information on the coupling of the photoelectron or the hole state to the surrounding medium. For photon energy below keVs the linear photon momentum plays usually no role, meaning the photon transfers only energy to the sample.

Dr. F. O. Schumann, Prof. J. Kirschner
Max-Planck Institut für Mikrostrukturphysik
Weinberg 2, Halle 06120, Germany
E-mail: schumann@mpi-halle.de

Prof. J. Berakdar
Institut fur Physik
Martin-Luther Universität Halle-Wittenberg
Halle 06099, Germany

The ORCID identification number(s) for the author(s) of this article can be found under https://doi.org/10.1002/pssb.201900636.

The electron momentum change required for the emission process is brought about by scattering processes from the potentials that bind the sample, for example, by recoiling off the ionic cores. If these ions are ordered in a crystal, only specific values of momenta, called crystal momenta, can be acquired by the photoelectron; a fact that can be used to map the electronic structure by simply accounting for the energy conservation law and recording the photoelectron angular distribution. For nonordered samples, such as amorphous systems or molecular aggregates, further measured quantities that relate to the momenta are needed, in addition to the energy balance to map out the spectral function of the sample. This can be done using electrons impinging onto the sample with a known energy and momentum and detecting two electrons that are released upon this scattering. If all vacuum electrons are fast, so as to minimize the final-state electron–electron interaction, and one tunes the detection system so as to focus on a single knock-out event of the initially bound electron, one can indeed measure the materials spectral function, as demonstrated by numerous experiments.[2–7] In principle, this technique is very general but very thin films are needed as the experiment is performed in a transmission mode. Also, very good energy and momentum resolution are desirable to resolve pertinent features in the spectral function, which might be a challenge when operating with very high impact electron energies. These complications can be remedied by conducting the experiments at somewhat lower energies and in the reflection mode.[8–13] In this case, further processes set in, however, that can be exploited to gain qualitatively new information. At low energies the two released electrons cannot be considered independent anymore due to charge- and current-density interactions as well as due to exchange, meaning that the scattering process cannot not be captured by an effective single-particle problem.

1.1. Two-Electron Emission via Single-Photon Absorption

The two-electron spectra embody two-particle information that in general cannot be trivially related or deduced from single-particle spectra, unless one chooses the electron energies and emission angles such that the electron–electron interaction is marginal and one focuses on a single process during which the incoming electron knocks out one further electron and the two electrons leave the sample without further scattering. Two electrons can also be released by a single photon (this process is called double

ADVANCED
SCIENCE NEWS
www.advancedsciencenews.com

physica pssb
status solidi
www.pss-b.com

photoelectron emission, DPE).[14,15] Again, the photon imparts only energy to the system but virtually no momentum. Intrinsic scattering processes in the sample lead eventually to the release of two time-correlated electrons.[16,17] An important caveat is that light–matter interaction in the regime of interest is a single-particle operator. Meaning, the photon can only be absorbed by one particle.[17] How the second particle is ejected then? Starting from the nonequilibrium Green's function theory, one can set up a formal theory to answer this question[18,19] in full generality. In essence, for weakly and moderately correlated materials one can identify the following mechanisms for DPE:

1.1.1. DPE1

One electron in the state $\epsilon^i_{\mathbf{k}_i}$ absorbs the photon with the frequency ω and propagates with, respectively, higher energy. Upon scattering from the crystal, the initial wavevector $\mathbf{k}_i$ is changed to $\mathbf{k}'_0$ by a multiple of the crystal momentum (we assume atomic units). Already at this stage the propagation may be diffusive due to electron–electron or electron–phonon scattering. These processes are widely discussed in single photoemission (SPE) spectroscopy which detects the photoelectron yield at the momentum $\mathbf{k}'_0$. In DPE however, the (intermediate) electron with $\mathbf{k}'_0$ excites another electronic state via the dynamic, nonlocal electron–electron interaction W, leading to two vacuum-state electrons with momenta $\mathbf{k}_1$ and $\mathbf{k}_2$. Thus, in this scenario, the photon acts effectively as an internal electron gun that generates electrons with an angular distribution which is roughly similar to the one known from SPE. How can we distill and what can we learn from this DPE mechanism? Imagine we calculate or measure the SPE angular distribution at the energy ω so that we know the distribution as a function of $\mathbf{k}'_0$ of the electronic state excited after photoabsorption. In DPE, we tune our detectors so as to register one electron with almost $\mathbf{k}_1 \approx \mathbf{k}'_0$. The other electron has then a much lower momentum $\mathbf{k}_2$. In this case the two electrons can be considered distinguishable, meaning that the direct scattering between the two electrons is dominant. The momentum transfer during this scattering is $\mathbf{q} \approx \mathbf{k}'_0 - \mathbf{k}_1$ which is small (as chosen by the experimental setup). In this case one can study the electron–electron interaction W in momentum space as a function of $\mathbf{q}$ at the energy $\omega - \epsilon^i_{\mathbf{k}_i}$. Such a study is particularly interesting if $\omega - \epsilon^i_{\mathbf{k}_i}$ happens to be near a plasmon resonance.[19–21] An experimental study confirming this picture and providing more mathematical foundations to it has been conducted recently.[19]

1.1.2. DPE2

The same process as (DPE1) but the fast intermediate electron, before or after scattering from the second electron, undergoes diffraction, which can be observed in this photoelectron distribution.[22] The diffraction pattern is as that known from SPE.

1.1.3. DPE3

With increasing $\mathbf{q}$ and hence $\mathbf{k}_2$ exchange scattering becomes more dominant, as the emitted electrons become indistinguishable. In addition, in contrast to processes (DPE1) and (DPE2)

Frank O. Schumann is an experimental physicist with research interests in electronics and magnetic properties of surfaces and thin films. He studied physics at the RWTH Aachen, Germany, and obtained the Ph.D. from Cambridge University, UK, in 1994. From 1994 to 1999, he was a postdoctoral researcher at Pennsylvania State University, USA, and Livermore National Lab, USA. From 1999 to 2004, he was a leader of a research group at the Free University Berlin, Germany. In 2004, he became a senior scientist at the Max-Planck-Institute of Microstructure Physics, Germany. In 2012, he obtained the Habilitation degree from the Martin-Luther University Halle-Wittenberg, Germany.

Jürgen Kirschner is an experimental physicist with research interests in electronic and magnetic properties of surfaces and thin films. He pioneered the development of spin-resolved electron spectroscopies and coincidence spectroscopy. He studied physics at the TU München, Germany, where he also obtained his Ph.D. in 1974. In 1982, he obtained his Habilitation degree from the RWTH Aachen, Germany. From 1975 to 1988 he was a staff scientist at Forschungszentrum Jülich, Germany. He was appointed as full professor at FU Berlin, Germany, from 1988 to 1992, before becoming founding director of the Max-Planck-Institute of Microstructure Physics Halle, Germany, in 1992.

Jamal Berakdar is a theoretical physicist with research interests in time- and spin-dependent processes in electronic many-body systems. He studied at the Universities of Heidelberg and Freiburg, Germany. He took a Ph.D. degree in 1994 from the University of Freiburg followed by a postdoctoral period at the Royal Holloway College, University of London and at the Australian National University, Canberra. From 1997 to 2006 he was a staff scientist at the Max-Planck-Institute of Microstructure Physics, Halle, Germany. Since 2006 he has been a full professor at the Martin Luther University, Halle, Germany.

the interaction between the two electrons becomes stronger as they approach each other in momentum space. Thus, in this case, one accesses higher-order electron–electron scattering events that contribute to W, resulting in the formation (in momentum space) of the exchange and correlation hole in the recorded two-electron spectrum.[14,15,23–25] As for exchange effects, we note that the light–matter interaction is not only a single-particle operator but also is symmetric with respect to

1900636 (2 of 14)

particle exchange. This means, a symmetric (antisymmetric) state is mapped onto the symmetric (antisymmetric) state via this interaction. In the absence of spin-orbit coupling the spin and orbital part of the wave function can be decoupled and the symmetry properties can be analyzed by just exchanging the momenta of the electrons (when operating in momentum space). These statements are strictly valid when the two electrons are emitted directly from the Fermi level but are less accurate when other secondary electrons are involved, for instance, when the two electrons suffer energy losses before being detected.

1.1.4. DPE4

This is the same as in (DPE3) but accompanied with diffraction from the crystal. Regardless of which of the electrons undergoes diffraction, because of nonnegligible exchange scattering, one can only observe a pair diffraction, meaning a change of the two-electron sum momentum by a multiple of the reciprocal lattice vector.[22]

1.1.5. DPE5

Interestingly, we can study the above mechanisms while allowing for a specific amount of energy and momentum dissipations to the sample, tuning so such loss mechanisms. This can be done utilizing the energy and momentum balances. To do that we detect the two electrons at energies and momenta that violate these laws. This implies that the missing energy and momenta have been absorbed by the surrounding medium via multiple inleastic scattering events that gradually randomize the phase relation between the electrons and degrade the strength of the two-electron flux density. An example for the consequences of such dephasing and decoherence is the "filling" of the exchange and correlation hole while allowing more and more for dissipation channels.[25] In the event that the exchange and correlation hole is filled a formulation of DPE in terms of the electron–electron interaction W is less meaningful.

1.1.6. DPE6

There is also a possibility that two mutually interacting electrons (such as a Cooper pair) absorb a photon and emerge with a zero total momentum, i.e., with back-to-back equal momenta[26] if both are launched from the Γ point.

1.2. Two-Electron Emission Following the Charged-Particle Impact

As stated above the electron–electron coincidence detection after a fast electron impact allows under certain conditions to access the spectral function $A(\omega, \mathbf{k})$, similar as for SPE but with the advantage that nonvertical transitions are allowed.[2–6] Hence, in some situations the electron impact and SPE should be related, a case known under the name the "optical limit" (meaning that the charged particle impact acts in this limit as a virtual photon). Note that the optical limit refers to SPE, not to DPE. The charged particle impact that is related in the optical limit to DPE is the one where three particles are detected in the final channel. For example, one very fast incoming electron leaves the sample after losing part of its momentum that is large enough to eject two further low kinetic energy electrons (a process called (e,3e)).[27] This process is indeed related to DPE in the optical limit. In fact the type of the charged particle is not relevant; it can be a positron or a proton. (The cross section in this case is quadratic in the charge of the projectile. The projectile mass and kinetic energy enter the cross sections as scaling factors.) From this perspective there is a clear difference between DPE and two-electron emission via particle impact (for electron impact, the process is usually referred to as (e,2e)), even though in both DPE and (e,2e) two electrons are released at the same time from the sample into vacuum. A series of studies have been conducted to unveil the various mechanisms involved in (e,2e) and the physics underlying them (for instance[8–12,28–31]). We discuss below prominent examples in the reflection mode (i.e., when all electrons are detected on one side of the film or surface).

1.2.1. e2e₁

The incoming electron is released from the electron gun with a momentum $\mathbf{k}_0$ and energy E_0 and is elastically (specularly) reflected back from the ionic background, acquiring the momentum state $\mathbf{k}_0'$. Upon an electron–electron scattering via W (the same W as in DPE), two vacuum electrons with momenta $\mathbf{k}_1$ and $\mathbf{k}_2$ emerge into the vacuum with energies E_1 and E_2. If a single scattering event via W is involved and if W is local then $\mathbf{k}_1 \perp \mathbf{k}_2$ (except for some corrections due to refraction at the solid/vacuum interface). The detection in this geometry delivers thus information on the nature of W and in particular its directional dependence. Note that in this mechanism $\mathbf{k}_1 \perp \mathbf{k}_2$ applies independent of the particular directions or energies of $\mathbf{k}_1$ and $\mathbf{k}_2$. These quantities can be scanned by simply varying the direction of the incoming electron momentum and/or E_1 and E_2. If this scattering process is dominant one may use the energy and momentum conservation laws (Φ is the work function) $E_0 - \epsilon_i - \Phi = E_1 + E_2$ and $\mathbf{k}_0' - \mathbf{k}_i = \mathbf{k}_1 + \mathbf{k}_2$ to map the electronic structure of the sample $\epsilon_i(\mathbf{k}_i)$. Clearly this type of extracting $\epsilon_i(\mathbf{k}_i)$ relies on more assumptions than its high-energy transmission-mode counterpart[2] but it has two main advantages. First, there is no need to fabricate very thin free-standing films (needed in the transmission mode) and one can use the detection techniques that are established in the field of low-energy electrons. Second, a more fundamental advantage is the extreme surface sensitivity at appropriate electrons' energy for two reasons: as two electrons have to leave the sample the escape depth is reduced significantly with respect to one single electron and second, the incoming or the outgoing electrons can be tuned to grazing angles, enhancing the scattering from the surface region.

1.2.2. e2e₂

A process absent in DPE is that the incoming electron may be affected already on its way to the surface by polarization and loss effects. A prominent example is the distortion of the incoming wave due to the image charge potential or plasmonic fields. The origin of these effects is mainly electronic and depends strongly on the detail of the electronic self-energy of the sample.

After scattering from the polarized surface charge the incoming electron may undergo further scattering events, resulting eventually in the emission of two electrons. Experimentally, this process can be distinguished[32] via the selected energy and momenta of the electrons, because the electronic response of the sample depends decisively on the transferred energy $\omega_{\mathbf{q}}$ and momenta $\mathbf{q}$. For instance, if we are interested in the plasmonic excitation by the incoming electron before the two final-state electrons are launched, we should tune appropriately $\mathbf{q} = \mathbf{k}_0 - \mathbf{k}_1 - \mathbf{k}_2$ and/or $\omega_{\mathbf{q}} = E_0 - \epsilon_i - \Phi - E_1 - E_2$. An interesting caveat is that one may use spin-polarized electrons and explore spin-dependent collective electronic response.

1.2.3. e2e₃

The e2e₂ in its intial step is the same as in electron-energy loss spectroscopy (EELS),[33] for instance, in both cases the incoming electron may excite a (multipolar) plasmon mode. At high momentum transfer $\mathbf{q}$ this mode merges with the particle-hole continuum. In EELS this decay leads usually to a particle-hole creation which is neutral excitation. In (e,2e) (and this mechanism we call e2e₃), the non-neutral (ionizing) regime is entered and the ejected electron is detected in coincidence with the escaping projectile (EELS) electron.

1.2.4. e2e₄

One or all of the electrons may undergo diffraction. Single-electron diffraction may be distinguished from electron-pair diffraction by tuning the electron energies. For example, if we are in the diffraction regime for one of the escaping electrons and $\mathbf{k}_1 \approx \mathbf{k}_2$ one cannot tell which electron is diffracted and indeed in the experiment one observes a diffraction with respect to the total momentum $\mathbf{k}_1 + \mathbf{k}_2$.

1.2.5. e2e₅

Exchange effects play in (e,2e) a markedly different role than in DPE.[28,30,31] This is evident if we consider a spin-polarized incoming electron from a magnetic or a spin-active sample. For an exchange-coupled magnetic surface with a weak spin-orbit coupling one finds under certain conditions that the measured two-electron signal is proportional to the product of the spin polarization vector of the incoming electron and the spin polarization of the sample at the energy (ϵ_i) and the wavevector dependent ($\mathbf{k}_1$). Combined with the surface sensitivity of the (e,2e) technique this observation allows to map the depth-dependent spin structure of ultrathin magnetic films.

1.2.6. e2e₆

Violation of the mechanism e2e₅ is a signature of spin-orbit coupling which might have different strengths at the various stages of the scattering process.[29,30] Even in the absence of spin-orbit coupling, exchange scattering is still operational, producing in general a statistical mixture of singlet and triplet cross sections. Exchange scattering is in fact an exchange of energies and wavevectors of the two electrons which appear as an exchange of spin. From this observation it follows that exchange scattering is generically large when $|\mathbf{k}_1|$ and $|\mathbf{k}_2|$ are comparable. In the case where the whole experiment (including the sample with its intrinsic symmetry) is invariant under the exchange of $\mathbf{k}_1$ and $\mathbf{k}_2$, the triplet-scattering amplitude vanishes.[34] In this situation the (e,2e) experiment produces singlet electrons only. For fixed $\mathbf{k}_1$ and $\mathbf{k}_2$ the orbital part of this state is also fixed. What can be done then is to measure the variation of the singlet cross section on the spin projections of each of the electrons and exploit the results to quantify the quantum entanglement. In this regard we note that the spin part of the singlet state can be viewed as a maximally entangled Bell state. The dependence of this entanglement on the orbital part can also be accessed by simply varying the impact energy and keeping the experimental setup such that the triplet scattering is zero.[31] Tuning the experiment where triplet scattering vanishes, both the exchange and the direct scattering amplitudes contribute. To "switch off" experimentally exchange effects one can use a positron instead of an electron as a projectile, as illustrated later. We recall in this context that only in the first Born or plane-wave approximations the scattering cross section does not depend on the sign of the projectile charge, so using the positron or electron as a projectile, one finds the same cross section in these approximations.

One can tune the energy of the incoming and the detected electrons such that ϵ_i corresponds to a core level in which case one enters the realm of resonant processes involving Auger decays. Some of the mechanisms outlined earlier are still operational. An example is given later.

2. Selected Results

Having listed the dominant mechanisms for the simultaneous ejections of two electrons upon photon or charged particle impact, we discuss below some important experimental details and prototypical results.

2.1. Experimental Section

Experimentally, identifying uniquely the two electrons that were emitted at the same time from the sample after one single-photon absorption or after the impact of one single charged particle is challenging and requires coincidence electronics. The fundamental obstacle is the very low cross section compared with single-electron emission. For DPE, when recording electron pairs due to single-photon absorption, one has to ensure that emission is not due to the absorption of two uncorrelated photons. It is customary to refer to these events as "random" coincidences whereas the events of interest are termed "true" coincidences. Regardless as to whether a continuous or pulsed source is used, the probability that two photons are within the coincidence window is determined by Poisson statistics. The primary flux determines the probability of finding two photons within the coincidence window. This probability scales quadratically with the flux, whereas the "true" coincidences scale linearly. Therefore one is forced to operate with a strongly reduced flux. Roughly speaking we need to throttle the incoming flux of a standard vacuum ultraviolet (VUV) source by more than three

orders of magnitude, making pair emission spectroscopy a time-consuming endeavor.

The main experimental work was carried out using a coincidence spectrometer described in detail in previous studies, see **Figure 1**.[35,36] The key components are a pair of hemispherical analyzers with 200 mm mean radius which we call "left" and "right," respectively. They are equipped with multichannel plate (MCP) detectors in which the impact position is determined by resistive anodes. For this instrument we have established a procedure which removes the "random" contribution from the measured spectrum. This yields the contribution of the "true" events, which we want to call "pair" intensity in the following paragraphs. As excitation sources an electron gun and a laboratory VUV source with a monochromator were available. To perform experiments with primary positrons we developed a low-energy positron beam which is based on the Na22 isotope.[37,38] A modified sputter ion gun allowed the excitation of the surface with low-energy He^+ and He^{2+} ions.[39–41] Studies on Auger decay were conducted at the synchrotron light source BESSY II of the Helmholtz-Zentrum Berlin (HZB). We comment briefly on a new DPE setup which uses a light source based on high harmonics generation in combination with a pair of time-of-flight spectrometers.[42–44]

2.2. Material-Dependent Intensity Relations

As outlined in the DPE processes (DPE1–DPE4) the intensity depends strongly on electron–electron interaction strength. A more quantitative statement can be made when using the Hubbard model with the electron–electron strength U. A previous study[45] identifies the experimental conditions under which the DPE intensity indeed scales with U. Generally, the Hubbard model and the U parameter for the electron–electron interaction is a mere theoretical model that needs to be adjusted to material-specific predictions. On the other hand, studies over the years identified the class of materials which can be called strongly correlated. Thus, one may attempt to compare the two-electron
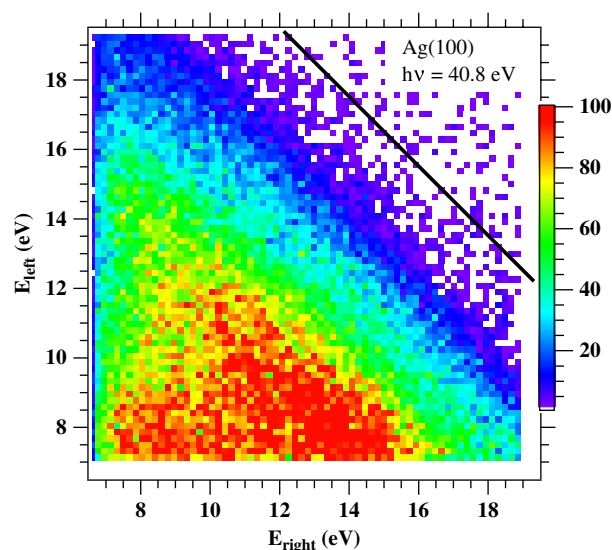

Figure 2. 2D energy distribution from a Ag(100) surface. The black diagonal line depicts the position of the maximum sum energy E_{sum}^{max}. The photon energy is 40.8 eV. Reproduced with permission.[46] Copyright 2016, American Physical Society.

yield from such correlated materials with those which are less correlated. In **Figure 2** we present a typical 2D energy spectrum from a Ag(100) surface whereas the photon energy was set to 40.8 eV. The diagonal black line marks the energetic position of the largest energy sum of a pair. We will label this entity with E_{sum}^{max}. Since in a DPE experiment two electrons are emitted the value of E_{sum}^{max} is determined by the photon energy minus twice the work function. Due to energy conservation there is no intensity above the E_{sum}^{max} line other than some "random" intensity. Although we explored a symmetric emission geometry, see Figure 1, the 2D energy plot is slightly asymmetric despite the fact that the emission geometry is symmetric. This is caused by some
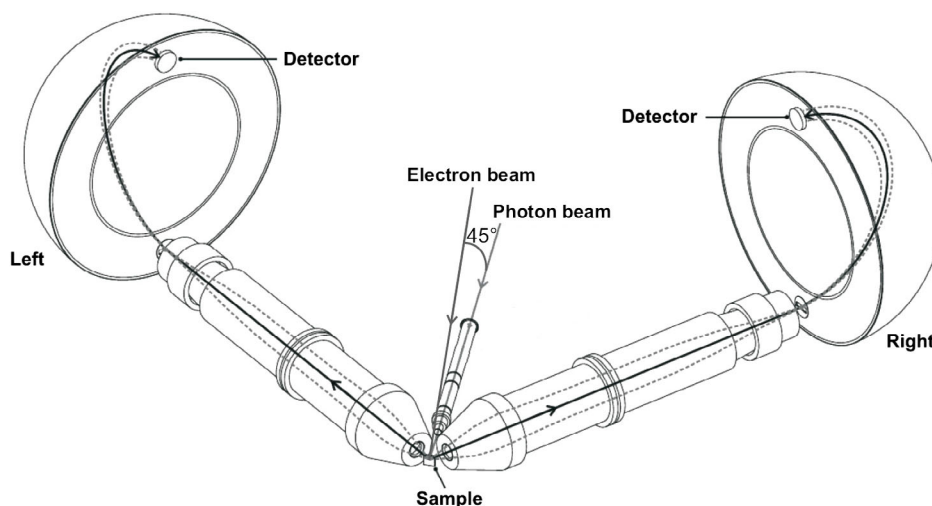

Figure 1. A schematic view of the coincidence spectrometer. Key components are two hemispherical electron spectrometers. The photon beam can be replaced by a low-energy ion source or positron source. The spectrometer axes include an angle of 90°. More details can be found in the literature.[35–38] Reproduced with permission.[46] Copyright 2016, American Physical Society.

misallignment of the transfer lenses of the spectrometer. The 2D energy spectrum does not exhibit any sharp features which to some extent is a consequence of the selected energy resolution. We will show later that the Ag(100) surface does display sharp features.[44] In this section the integrated intensity within the 2D energy window is of interest. Therefore, trading in intensity on the expense of energy resolution was warranted. For each material only a measurement time of 1 h was required to determine the count rates with sufficient accuracy. The data were obtained in several experimental runs. Upon start-up of the instrument we noticed daily variations of the rates from the Ag(100) surface. These variations were on the scale of 10%. We therefore normalized the rates of the various materials with the rates of the Ag surface each day. These normalized rates were scaled with the average rates of Ag from the different measurement days.

In **Figure 3**a we show the result for the DPE intensity as a function of the singles rate. The lowest singles rate was observed for V which is roughly a factor of 3 smaller that for NiO. At the same time we note that the coincidence rate for NiO is a factor of 8 larger than the value for V. Without the data points of the ferromagnets an almost monotonic variation of the coincidence rate
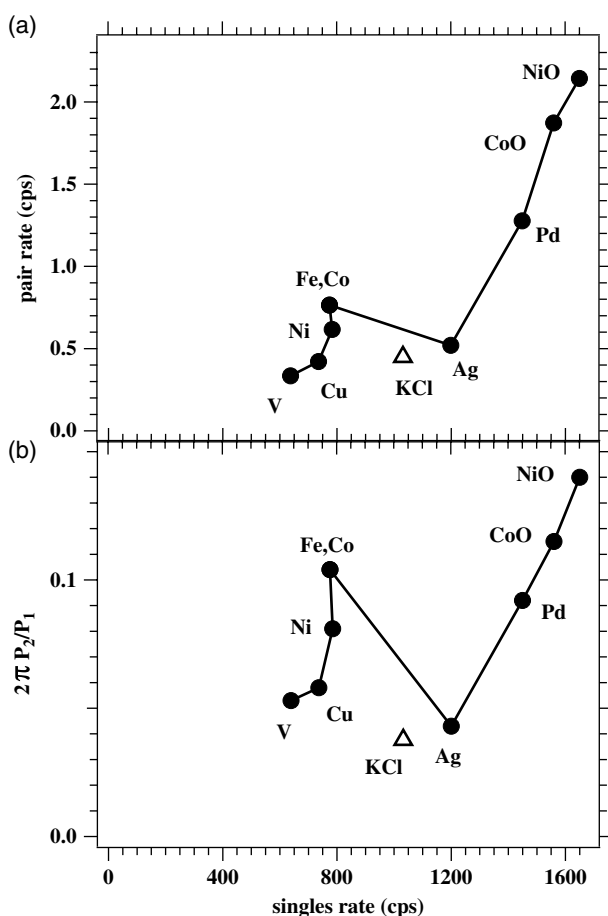
as a function of the "singles" rate can be seen. The transition metal oxides NiO and CoO display the highest "pair" rate, this supports the theoretical prediction that the pair emission rate scales with the electron correlation strength.[45] We also investigated a KCl single-crystal surface. We ensured the same kinematics by increasing the photon energy to 48.4 eV. This takes into account the different work functions for Ag and KCl. In addition we changed slightly the spectrometer settings to include essential parts of the energy spectrum. KCl is an insulator like NiO or CoO but does not possess the intensity level of these oxides. Obviously the reasoning of an increased mean free path in insulators which in turn increases the number of layers probed in a DPE experiment does not hold. The higher intensity level of NiO and CoO is a reflection of the stronger electron correlation rather than its insulating properties.

A closer look at the ferromagnetic samples reveals that one measures about 65% of the Ag "singles" rate but up to a factor 1.5 higher "pair" rate. This means that the ratio of the "pair" rate to the "singles" rate is significantly higher than that for Ag. We make the following definitions. The probability for one electron to be emitted within a solid angle interval ranging from Ω to $\Omega + d\Omega$ is given by $P_1(\Omega)d\Omega$. The equivalent for pair emission is the term $P_2(\Omega_A, \Omega_B)d\Omega_A d\Omega_B$. This describes the joint probability that one electron is emitted in a solid angle range centered at Ω_A whereas the other electron emission direction is characterized by Ω_B. In our definition the term $P_1(\Omega)d\Omega$ includes also electron pair excitation, but the second electron is not emitted. In our previous measurements we have identified a distinct angular dependence of the coincidence intensity. Therefore the terms P_1 and P_2 are angle dependent. The angular range covered by the instrument used here allows to use an angular averaged value.[46] In the following P_1 and P_2 are constants.

For the probability s to detect one electron we can write

$$s = \int (P_1 + 2\pi P_2)d\Omega_A = P_1\left(1 + \frac{2\pi P_2}{P_1}\right)\Omega \tag{1}$$

The factor of 2π in front of the term P_2 takes into account that the second (but undetected electron) is emitted somewhere within the half sphere. The probability t to detect an electron pair with two identical spectrometers is

$$p = \int P_2 d\Omega_A d\Omega_B = P_2\Omega^2 \tag{2}$$

Simple arithmetic yields the relation

$$\frac{2\pi P_2}{P_1} = \frac{2\pi}{\Omega \cdot s/t - 2\pi} \approx \frac{2\pi}{\Omega}\frac{p}{s} \tag{3}$$

The term $2\pi P_2/P_1$ is a measure of the contribution of pair emission to the detected single-electron spectrum, see Equation (1). The factor 2π takes into account that the second (undetected) electron is emitted somewhere in the half space. The ratio s/p is identical to the experimental count rates for "singles" and "pair" events. For a Ag(100) surface this ratio is 2400, whereas the solid angle of our spectrometer is about 1% of 2π. Therefore the denominator can be approximated by the first term. This means the ratio of "pair" to the "singles" rate determines the fraction of the pairs to the "singles" spectrum. In the evaluation we have used the correct term as shown in

Figure 3. Panel a) shows the DPE intensity as a function of the singles rate for a variety of materials obtained with $h\nu = 40.8$ eV. The data point for KCl was measured with $h\nu = 48.4$ eV. Panel b) displays the variation of the entity $2\pi P_2/P_1$, as explained in the text. Reproduced with permission.[46] Copyright 2016, American Physical Society.

ADVANCED SCIENCE NEWS
www.advancedsciencenews.com

pss b
physica status solidi
www.pss-b.com

Figure 3b. Clearly the curve resembles Figure 3a in the shape but demonstrates the interesting point that 5–15% of the "singles" emission is due to pairs. This means that DPE at surfaces is a rather efficient process. In the presentation of Figure 3b the signal levels of the ferromagnets Fe, Co, and Ni are significantly higher than Ag. This is a reasonable result because ferromagnetism is a manifestation of electron correlation. This suggests that the term $2\pi P_2/P_1$ may be better suited for the quantification of the correlation strength.

We have conducted the equivalent study via (e,2e) together with the DPE measurement in an interleaved mode.[46] Again the material with the highest coincidence count rate is NiO which is about a factor of 15 larger than for Cu which has the lowest coincidence rate. At the same time the singles rate for NiO is a factor of 3.5 larger than for Cu. Similar to the DPE data we notice an almost monotonic relation between the coincidence and singles rate. Evaluating the term $2\pi P_2/P_1$ for NiO reveals a value of 40%. Also in (e,2e) the emitted pairs make a substantial contribution to the singles rate. The measurements were carried out at room temperature. The ordering temperature of the ferromagnetic and antiferromagnetic samples was well above the measurement temperature except for CoO films. From our previous studies we have determined that measurements above and below the Neel temperature of NiO and CoO films display the same singles and pair count rate.[46,47] This means that our type of spectroscopy is not sensitive to long-range order but is determined by the local correlation.

2.3. Positron–Electron Pair Emission

The exchange-correlation hole, discussed above, has indeed been experimentally observed.[25,48] Using spin resolved (e,2e) from the ferromagnetic sample it is possible to study exchange effects.[49,50] As eluded to in the beginning one can switch off completely exchange effects during scattering using positron impact.[51,52] This pair emission due to the impact of a primary positron beam is termed (p,ep).

We established the existence of a finite (p,ep) intensity using a positron beamline at the research reactor FRM-2.[35] This warranted the development of a laboratory positron beam as described in previous studies.[37,38] This facility has an intensity of about 40 000 e$^+$/s which is roughly two orders of magnitude below the value before "random" coincidences become dominant. Therefore we operated the spectrometer with the largest entrance slits to obtain reasonable count rates. The consequence was an energy resolution of 5.1 eV per spectrometer.[53]

In **Figure 4** we highlight the geometry of the experiment. The primary positron beam and the electron-optical axes of the spectrometer define a scattering plane. The surface normal is within this plane and points toward the positron beam. The spectrometers are symmetrically arranged with respect to the surface normal. In the following we want to call one of them "left" whereas the other is labeled "right." Reversing the polarity of the voltages applied to the electron-optical components of one spectrometer allows the detection of positrons with this spectrometer, whereas the other will record electrons.

Let us assume that we want to record electron pairs due to primary electron excitation using the symmetric arrangement
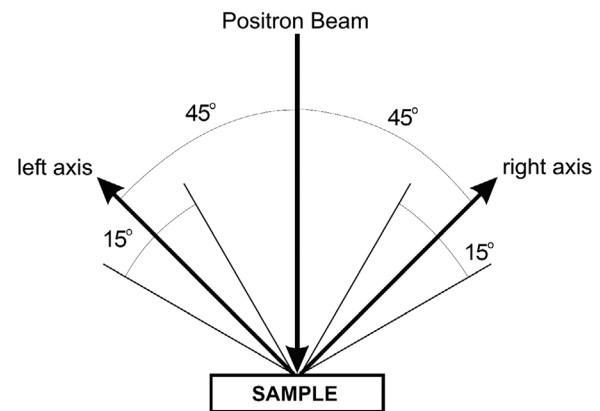

Figure 4. Geometry of the (p,ep) experiment. A primary positron beam is parallel to the surface normal. The transfer lenses are symmetrically oriented to the left and right of the incoming beam. Reproduced with permission.[37] Copyright 2014, American Physical Society.

of Figure 4. We further assume that the energies of the outgoing electrons E_1 and E_2 are different. The chances of the electron with energy E_1 to be detected by the "left" spectrometer are equal to the detection at "right". This is an immediate consequence of the nondistinguishability of electrons. The detection of a positron–electron pair will break the symmetry and therefore we expect an asymmetry in the energy distributions. The question which arises is then how much is the asymmetry and how it is affected by the actual material. We start with the example of a Ag(100) surface which was excited by a primary beam with 42 eV. The resulting 2D energy spectra are plotted in **Figure 5**. The insets highlight the chosen polarity of the spectrometer. The x-axis in both cases is the energy scale mapped by the "right" spectrometer, whereas the y-axis is the energy of the particles detected with the "left" spectrometer.

The solid diagonal line in both plots marks the position of the maximum sum energy E_{sum}^{max} which is given by the primary positron energy minus the (electron) work function. There is some tailing of intensity above this line which is due to the degraded energy resolution. Most of the intensity is found within a triangular-shaped region near the lower left-hand corner. This is caused by further collisions of the positron–electron pairs. The energy loss incurred in these processes can be sufficient to cause the emission of a second electron. We are unable to detect the emission of two electrons and a positron, but we observed electron pairs due to positron impact.[53] This strongly suggests the existence of triple emission. This effect is not part of the theory of (p,ep). If we want to invoke the symmetry of the detection geometry one has to exclude the contribution of these events. This can be facilitated via an appropriate selection of the sum energy. The pair of dashed lines indicates the range considered for the computation of the energy-sharing curves, see later. Even without the sharing curves an asymmetry is immediately noticeable in Figure 5a if we focus on the region marked by the dashed lines. Within this region the intensity is higher in the upper left-hand region compared with the lower right-hand part. We changed the polarities of the spectrometers and observe in Figure 5b that the region of higher intensity is now in the
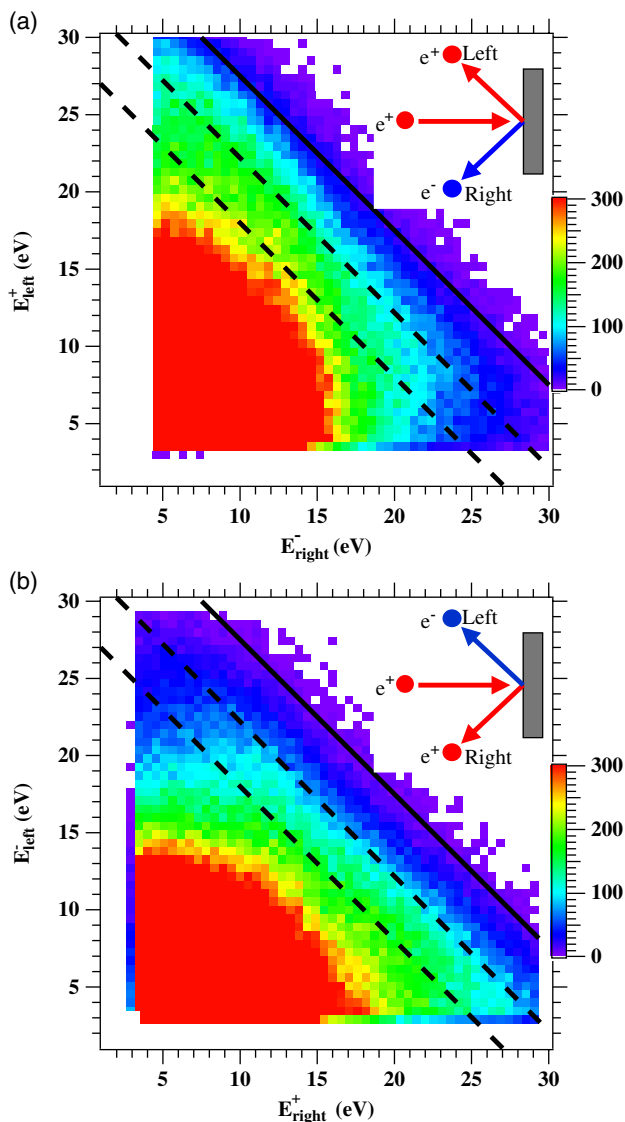
Figure 5. 2D energy distribution of positron–electron pairs from the Ag(100) surface. The primary energy was 42 eV. The insets indicate which of the particles is detected by the respective spectrometer. The x-axis in both plots refers to the energy measured by the "right" spectrometer. In panel (a) the "left" spectrometer was tuned to positron detection whereas in (b) it is the "right" spectrometer. Reproduced with permission.[37] Copyright 2014, American Physical Society.

Figure 6. Energy-sharing curves obtained by fixing the sum energy to 30 ± 2 eV. The Ag, Co, and NiO samples were excited by 42 eV positrons. The insets indicate which of the particles is detected by the respective spectrometer. Reproduced with permission.[37] Copyright 2014, American Physical Society.

lower right-hand corner. This rules out an instrumental asymmetry as the major cause. A control experiment with an electron gun in a symmetric geoemtry shows that the resulting (e,2e) sharing curve is essentially symmetric.[37] The dashed lines in Figure 5 define a region of the sum energy in the range $E_{sum} = 30 \pm 2$ eV. The events selected by this choice can be shown as an intensity curve as a function of the energy difference $E_{left} - E_{right}$, see **Figure 6**. If one reverses the polarity of the spectrometers the intensity maximum moves from right to left. In Figure 6a most of the intensity is found for positive x values. This means that on average the positron has a higher fraction of the available energy. The intensity maxima of the two (p,ep) sharing curves are
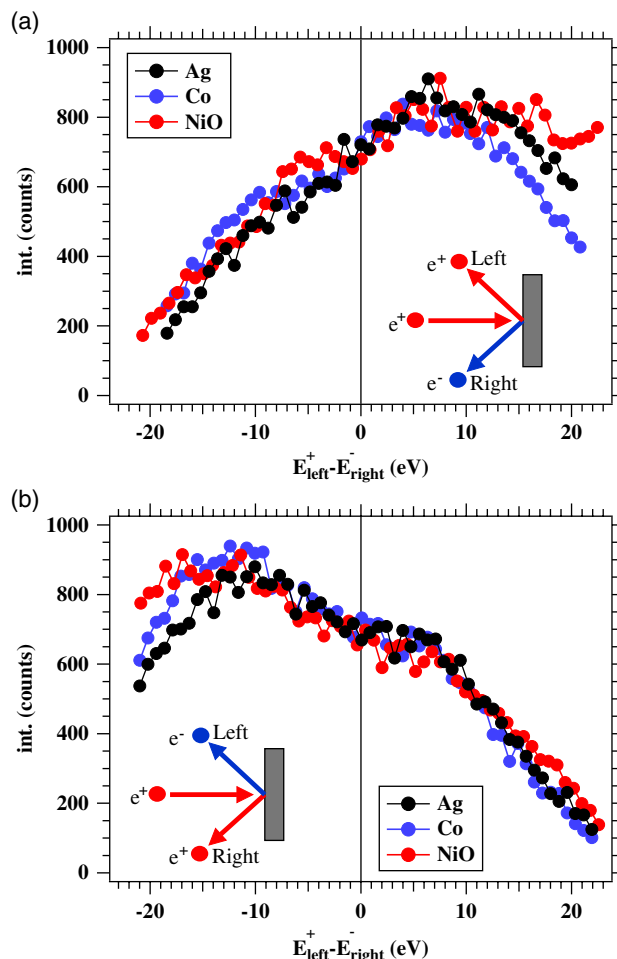
observed if the positron has 10 eV more energy than the electron. The intensity has the lowest value if the electron has a 20 eV higher energy than the positron. The intensity ratio between these two levels is roughly 4. We tested the generality of these observations and prepared single-crystalline NiO, Pd, and Fe films. In addition, we prepared polycrystalline Co, Ni, and Fe films. We have included the data of Co and NiO in Figure 6. For the purpose of comparison we scaled the intensity of the Co and NiO data such that they line up for equal energy sharing with the Ag data. An effective single-particle picture works well to describe the material properties of Ag. Co and NiO both display long-range order, this is a manifestation of electron correlation via the exchange interaction. NiO is an insulator, a property decisively determined by electron correlation. Despite these differences in the material properties and crystalline order the amount of the asymmetry in the sharing curves varies only slightly between the materials. Common to these samples is that on average the positron carries more energy than the electron. Although the sharing curves closely resemble each other the

ADVANCED SCIENCE NEWS
www.advancedsciencenews.com

pss b
physica status solidi b
www.pss-b.com

actual coincidence count rates differ strongly between these materials as shown in (e,2e) and DPE experiments.[46,54] Our observations were not a priori expected. Theoretical (p,ep) calculations suggest that depending on the valence state involved either the electron or the positron is the more energetic particle.[51,52] Details of the valence band structure determine the outcome, but no simple argument can be put forward.

For a qualitative understanding we developed a simplified scattering model. We reduced the problem to a two-particle model.[37] The interaction between positron and electron is mediated by a screened Coulomb interaction as it is in the current (e,2e) and (p,ep) theory. As screening length we adopted a value of 2 Å consistent with what is being used in actual calculations. The primary energy was set to 30 eV and we determined the scattering amplitude f(θ) within the first Born approximation. We obtained a sharing curve shown in **Figure 7**. Despite its simplicity it captures the essential feature that on average the positron has a higher kinetic energy compared with the electron.

During the coincidence measurements three different rates are measured by the electronics. These are the singles rate of the "left" and "right" spectrometer. In addition there is the "pair" rate. With the additional knowledge of the primary positron flux we normalize the actual rates. With this analysis we present the material dependent intensities in **Figure 8**. All measurements were carried out with a primary energy of 42 eV. The data are the average of two measurements in which either the left or right spectrometer was tuned for positron detection. In this figure we plot the coincidence rate versus the electron count rate (red data points) and the positron count rate (blue data points). It is clear that the coincidence rate for NiO is by a factor 2–3 larger than that from the metal samples. We also note an almost monotonic relation between the coincidence and singles rate. This resembles the result for DPE shown in Figure 3a.

While the singles rate varies by a factor of 1.9 the coincidence rate scales by a factor of 1.5. For a given material the electron singles rate is a factor of 2–3 larger than the corresponding positron rate. One can understand this in a simple picture. A primary positron can create secondary electrons as primary electrons, the
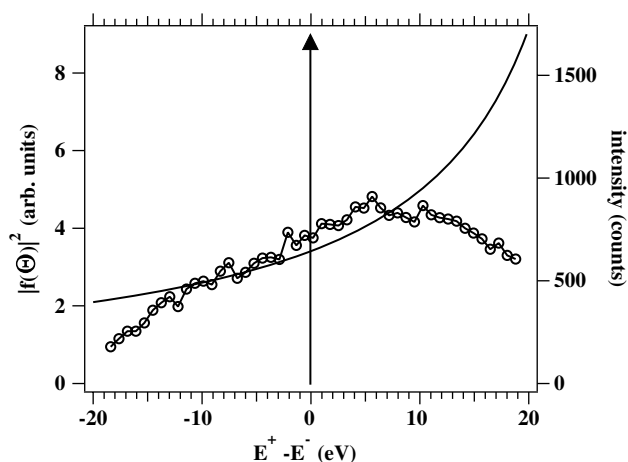

Figure 8. Coincidence rate as a function of the single-particle rate. Both rates are normalized to the incoming flux. The solid curves are guides for the eye. Reproduced with permission.[38] Copyright 2015, American Physical Society.

actual secondary yields are comparable. However, secondary positrons cannot be emitted, because the chance for two or more positrons to be present in the sample is essentially zero.

2.4. Ultrafast Auger Decay

The absorption of a photon can lead to the emission of an electron pair. We have termed this process DPE. It is worthwhile to discuss the simplest case which is the He atom. To create a He^{2+} ion the photon energy has to be larger than 79.01 eV. The energy above this value defines the energy sum of the pair which is shared continuously between those electrons. This leads to the schematic 2D energy distribution labelled one step in **Figure 9**b.

If a photon is absorbed by a core-level electron it may be emitted, which provides an important tool for the chemical analysis of surfaces via X-ray photoemission spectroscopy (XPS), because the kinetic energy is element specific. The rearrangement of

Figure 7. The solid curve is the sharing distribution $E^+ - E^-$ obtained within our simplified scattering model. The data points stem from the Ag data shown in Figure 6a. Reproduced with permission.[37] Copyright 2014, American Physical Society.
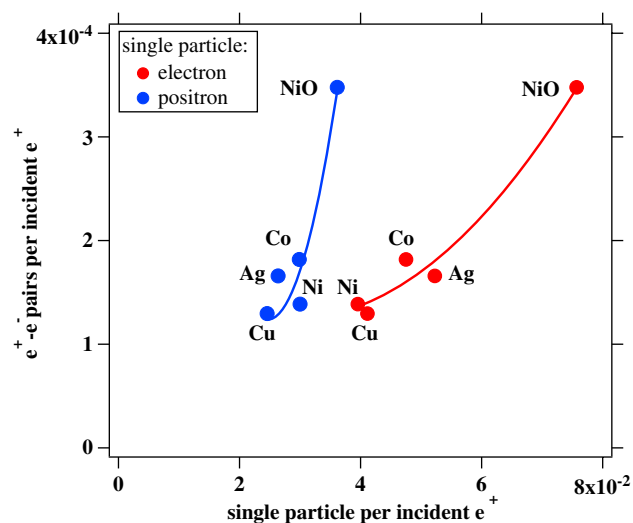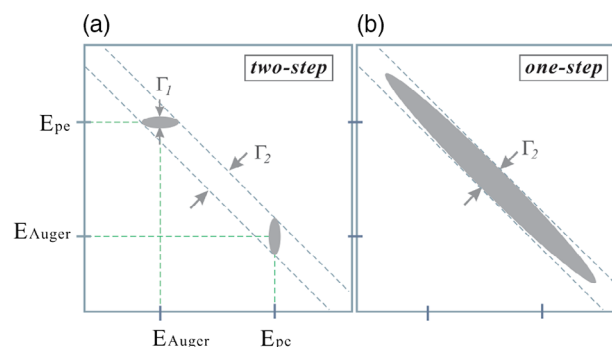

Figure 9. A schematic of 2D energy distribution for a two-step and one-step absorption process. Reproduced with permission.[55] Copyright 2014, American Physical Society.

charges leading to the filling of the core hole causes the emission of Auger electrons whose kinetic energy is also element specific. These two steps are usually considered to occur sequentially. Therefore we expect an energy distribution with intensity regions parallel the x- and y-axis, as shown in Figure 9a.

Let us consider the Auger decay of a Ag(100) surface. We will focus on the excitation of two different core levels. The subsequent Auger electron emission is due to the rearrangement of valence electrons. We used the instrument introduced in Figure 1 and utilized synchrotron radiation. More experimental details can be found in previous studies.[55,56]

In **Figure 10** we show the 2D energy spectra if either the $3d$ or $4p$ level is excited. The photon energy of the $3d$ experiment was 739 eV which ensured the both the $3d$ photoelectron and Auger electron are within the energy window of each spectrometer. The photon energy for the $4p$ experiment was set to 118 eV. For both experiments the sample has a final state characterized by two vacancies in the valence band. In both plots we have added dashed diagonal lines which mark the position of E_{sum}^{max}. The value is determined by the photon energy minus twice the work function. In addition we have divided the 2 E energy window into three regimes termed I, II, and III. The boundaries, given by the solid diagonal lines, have the same energetic distance to the E_{sum}^{max} line in both panels. In panel a) we observe that the photo electrons lines are separated by the spin-orbit interaction, the energetic position is at 366.6 and 360.9 eV, respectively. Due to the spin-orbit splitting there exist two Auger lines at 347.3 and 353 eV, respectively. While the photoelectrons are relatively narrow the Auger lines are considerably broader. Since the filling of the core vacancy involves two electrons in the valence band the self-convolution of the density of states (SCDOS) explains the line width of the Auger lines. The largest fraction of the intensity lies in region II. The arrangement into intensity bands either parallel to the x- or y-axis is in line with the sketch of Figure 9a.

A very different behavior shows up in Figure 10b. The key feature is a strong intensity residing within region II but is along a diagonal direction. This is the outcome shown in Figure 9b. This means the $4p$ decay does not proceed within a two-step process but is of a one-step type.

Let us recall known facts on the $4p$ line width of elements in the neighborhood of Ag in the periodic table. For those elements the $4p$ line width is extraordinarily large.[57–59] Autoionization is the electron emission of an excited sample which changes the charge state. The Auger effect is such a process. The explanation of the $4p$ line width rests on the use of two-electron configurations within a single-particle description. One configuration is continuous in energy, the other is discrete. In the presence of a finite electron–electron interaction the single-electron description is only approximate. A first correction is the introduction of the configuration interaction as introduced by Fano.[60] It turns out that the characteristic time for the autoionization process is inversely proportional to the interaction strength. When applied to the case of the Ag $4p$ decay a $4p^{-1}$ and $4d^{-2}4f$ configuration play the important role. The first is a discrete configuration and the latter the continuous one. The ionization of the $4p$ level requires an energy of 60 eV. The creation of a double vacancy in the $4d$ band while populating a $4f$ level, an energy within a window of 53 ± 13 eV is needed.[55,61] Consequently the two configurations overlap in energy. This is the origin of a rapid fluctuation $4p^{-1} \rightleftharpoons 4d^{-2}4f$, leading to a broad $4p$ line width.

The process of electron-pair emission upon absorption of a single photon has to obey energy conservation. This means the energy sum has to be conserved which in a 2D energy plot that defines a diagonal region. This relation can only be observed in coincidence spectroscopy. It is clearly manifested in Figure 10b that the main intensity is confined within a diagonal band with a width of 35 eV. Measurements with different photon energies showed a width of the diagonal feature of 11–38 eV. If we were to take the smallest width and use the energy-time uncertainty relation we end up with a timescale of 60 as. This characterizes the timescale of the correlated electron emission.
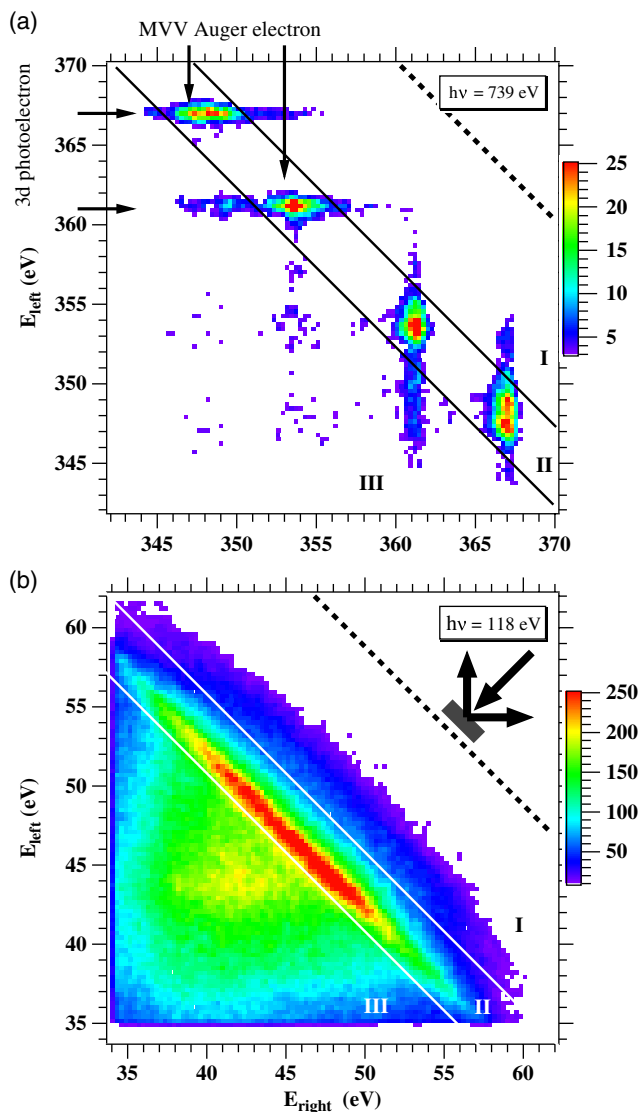

Figure 10. 2D energy spectrum from Ag(100) surface. In (a) the $3d$ level is excited whereas in (b) the $4p$ level is excited. The photon energies are 739 and 118 eV. The dashed diagonal lines mark the position of the maximum sum energy. Reproduced with permission.[55] Copyright 2014, American Physical Society.

2.5. Pair Emission Due to He^{2+} Neutralization

Suppose two photons impinge onto a sample within a short time interval, does the system respond as if two independent quanta are absorbed or will it consider the two quanta as one unit. This conceptional simple question was addressed in a calculation dealing with the two-photon double ionization of the He atom.[62,63] The photon energy was fixed to 70 eV; therefore, the creation of a He^{2+} ion requires two photons, because the double ionization energy is 79.01 eV. If the temporal width of the photon beam is larger than 4.5 fs the two emitted electrons possess well-defined energies. This is indicative of two-step ionization. However, if the temporal width is 300 as then the available energy is shared by the electron pair. In other words the system reacts as if a single energy quantum with 140 eV has been donated. This opens the potential to derive the characteristic time τ for correlated electron dynamics.

Although the theoretical example concerns an atomic target it is equally interesting to investigate condensed matter specimens, e.g., surfaces and thin films. Invariably an intense photon beam is at odds with the requirements of coincidence spectroscopy as outlined earlier. Nevertheless it is possible to conduct an equivalent experiment. Our approach is based on the well-known phenomenon of neutralization of an ion near a metal surface.[64–66] If an ion approaches the surface neutralization takes place at around 2-6 Å in front of the metal.[67–69] It is essentially an Auger-type process, as shown in **Figure 11**. A singly charged ion is close to a surface and the atomic energy levels experience a shift (2 eV) due to the action of the image charge. A valence electron can make a transition into the projectile level. This is followed by a radiationless transition of energy which causes the emission of a metal electron. This process is called Auger capture, there exist additional possibilities for neutralization. A doubly charged He^{2+} will become a neutral atom after two successive steps in which two energy quanta become available.[67,68]

From the literature one derives the average time between these steps of 2–20 fs.[67–69] The key point is the possibility to
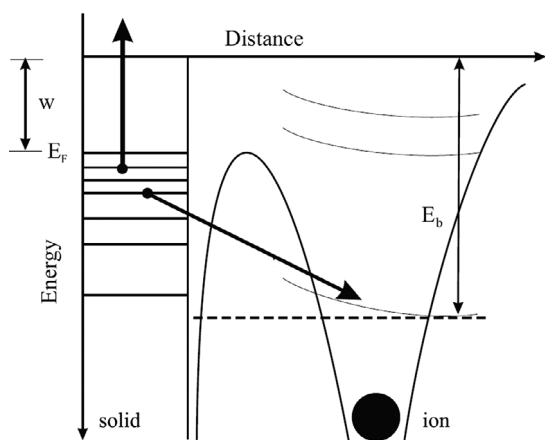
Figure 11. Neutralization step via Auger capture of a singly charged ion in the vicinity of a metal surface. A metal electron makes a transition into the lower-lying level of the ion. The energy gain leads to electron emission from the metal. Reproduced with permission.[41] Copyright 2017, American Physical Society.

obtain two energy quanta within the range of interest covering 300 as–4.5 fs. Additional encouraging facts are the high efficiency of neutralization. Almost all ions are converted into atoms after interaction with the surface. Furthermore, the electron yield for He^{2+} is 0.8 electrons per ion. This suggests a high chance to actually detect the emission of electron pairs.

If the kinetic energy of the He^{2+} ion is below 100 eV it can be ignored in the energy considerations.[70] The key entity is then the double ionization energy of 79.01 eV. This can be facilitated by a single photon. On the other hand, one can ionize the atom to He$^+$ after supplying an energy of 24.59 eV, which is followed by a second ionization step requiring 54.42 eV. With these values we discuss the energetics of neutralization. The first neutralization step from He$^{2+} \rightarrow$ He$^+$ which includes electron emission can be written as

$$M + \text{He}^{2+} \rightarrow M^{2+} + \text{He}^+ + e^- \qquad (4)$$
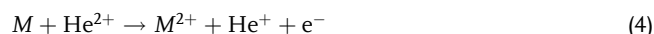
As we can see the metal M donates two electrons, one changes the charge state of the ion whereas the other is emitted. Consequently the maximum energy of the emitted electron is determined by the ionization energy minus twice the work function of the metal. For a Ir(100) surface the numerical result is 42.9 eV. For the neutralization He$^+ \rightarrow$ He^0 we obtain

$$M + \text{He}^+ \rightarrow M^{2+} + \text{He}^0 + e^- \qquad (5)$$

Also in this case the metal donates two electrons, one of which is emitted. We have to correct again twice the work function to determine the maximum energy of the second emitted electron. For a Ir(100) surface we obtain a value of 13.07 eV. After the completion of the two steps the maximum energy of the emitted pair is 55.97 eV for the Ir(100) surface.

It turns out that He^{2+} neutralization is accompanied by the electron-pair emission which is by no means a trivial point.[41] In **Figure 12** we show the 2D energy distribution obtained from a Ir(100) surface with an incoming He^{2+} beam of 10 eV kinetic energy. An L-shaped region is defined by the red boundaries. In one energy direction the kinetic energy cannot exceed 42.9 eV whereas in the other direction it is limited to 13.07 eV. These are the energy values we just introduced in the discussion of a sequential neutralization. The dashed diagonal lines in both panels indicate the position of $E_{\text{sum}}^{\text{max}} = 55.97$ eV of pairs. For the data shown in Figure 12a both spectrometers were set to a central energy of $E_k = 19$ eV. We notice the largest intensity if both electrons are below 10 eV. The largest part of the intensity can be found within the L-shaped region. This means the two neutralization steps leading to the He atom proceed mainly independently. Nevertheless we observe some intensity outside the L-shaped region. From this we can conclude immediately that there is another mechanism leading to pair emission. If we set $E_k = 30$ eV the coincidence spectrometer can only detect events which are outside the L-shaped region, see Figure 12b. These events are at odds with sequential emission. The intensity is highest if both electrons have an energy at the lower part of the detection window. The intensity gradually decreases if one moves closer to the dashed diagonal line. However, a cutoff value where the intensity drops sharply cannot be identified.[41]

A closer look at the intensity levels of Figure 12a reveals that outside the L-shaped region only 2% of the total intensity is
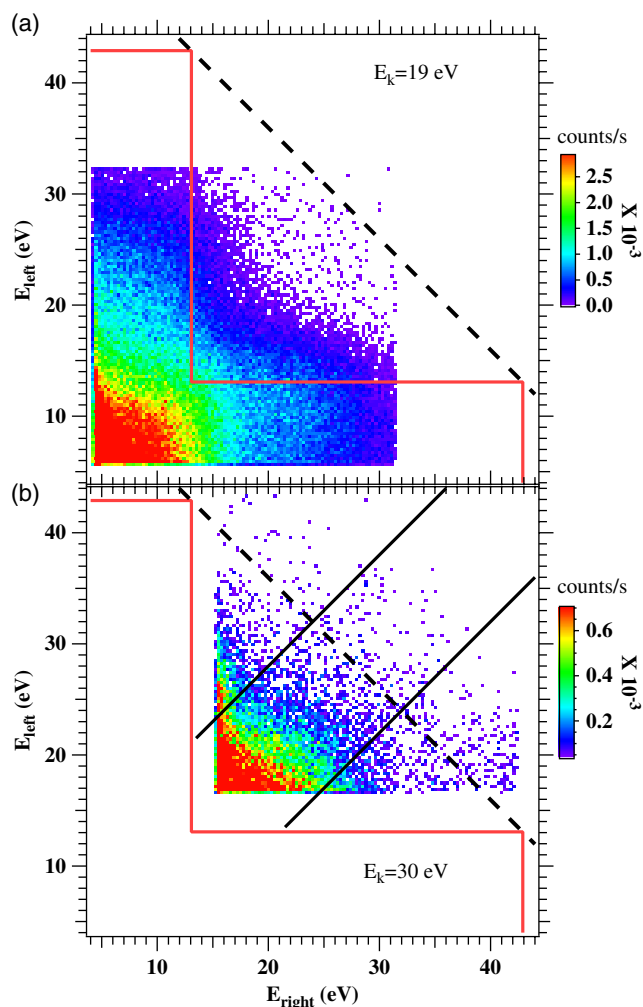
(a)

(b)

Figure 12. 2D energy spectra for a central energy of $E_k = 30$ eV from a Ir(100) surface. The kinetic energy of the He^{2+} ions is 10 eV. Emitted pairs which are due the sequetial emission mostly reside within the L-shaped region. The dashed black diagonal lines mark E_{sum}^{max}. The pair of black solid lines in the region $|E_{right} - E_{left}| \leq 8$ eV used for the E_{sum} spectrum. Reproduced with permission.[41] Copyright 2017, American Physical Society.

found. With this information we propose a simple picture to estimate the time scale τ for the correlated electron emission. The two neutralization steps occur on average within a time t_{avg} and we assume that they proceed independently. The small intensity contribution outside the L-shaped region indicates that $t_{avg} \gg \tau$. The probability for the two neutralization steps to occur within a time interval τ is then given by the Poison distribution $P(\tau/t_{avg}) \approx \tau/t_{avg}$. If the intensity contribution outside the L-shaped area is a measure of t_{avg}/τ, we obtain $\tau = 0.02 \cdot t_{avg}$. We adopt for t_{avg} values in the range 2–20 fs on the basis of the neutralization rate[67–69] This finally yields to $\tau = 40$–400 as. Hence, two formally independent neutralization steps occurring within an interval shorter than τ are recognized as a single excitation for electron-pair emission.

We propose a simple picture which explains the one-step process. If a core vacancy is filled by an electron, the available energy
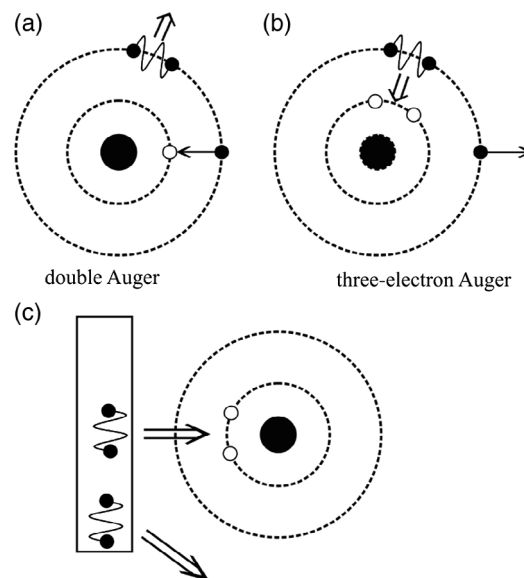
(a)   (b)

double Auger   three-electron Auger

(c)

Figure 13. In (a) a core hole is filled by an electron and pair emission called double Auger decay takes place.[71] In the three-electron Auger (b) a double vacancy is filled by an electron pair, the gained energy is transferred to a third electron.[72,73] In (c) an electron pair of the metal fills the double vacancy and an electron pair from the metal is emitted. Reproduced with permission.[41] Copyright 2017, American Physical Society.

can be transferred to not one but two electrons, see **Figure 13**a. This double Auger decay has been observed in coincidence spectroscopy from Ar.[71] A three-electron process takes place if a double core hole is filled by an electron. The available energy is then transferred to a third electron which is emitted, see Figure 13b. This leads to a kinetic energy which is roughly twice the regular Auger energy. This process was observed in C- and N-ion collisions with Ni surfaces and carbon foils.[72,73]

Let us combine these pathways, as shown in Figure 13c. Upon approaching the surface the double vacancy of the He^{2+} ion is filled by two electrons reminiscent to the three-electron Auger. The key difference is that these electrons do not originate from the higher lying orbitals of the atom but come from the surface. The energy gain is transferred to an electron pair of the surface which is emitted. This view is further corroborated by a recent work in which the electron capture for He^{2+} ions into excited states proceeds in a single step.[40] Extending this picture of a correlated double-electron capture, we observe here a single step of an electron pair from the metal into the ground state of the He atom.

2.6. Band-Resolved Double Photoemission

Double photoemission experiments without synchrotron radiation are possible with standard laboratory sources. Unfortunately these limit the available photon energies to a few lines. An alternative path uses the high harmonic generation of noble gases. We have developed such a light source with the required high repetition rate in the MHz range.[42] This provides lines covering 20–40 eV photon energy, and this source has been adapted to a setup incorporating two time-of-flight spectrometers.[43] The overall geometry is identical to the instrument shown in Figure 1.
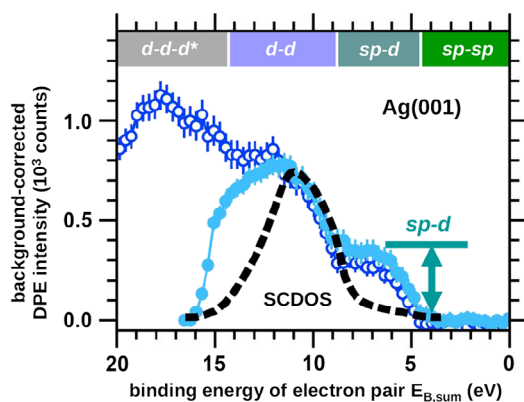
Figure 14. Sum energy spectra from a Ag(100) surface with a photon energy of 32.3 (25.1) eV for the empty (solid) symbols. The black dashed curve is the SCDOS. Reproduced with permission.[44] Copyright 2017, American Physical Society.

The improved energy resolution compared with the studies discussed earlier is manifested in a sum energy spectrum which displays a fine structure, see **Figure 14**.[44] In this experiment the photon energies were 32.3 and 25.1 eV, respectively.

The dashed black curve is the SCDOS. Since two electrons are removed from the valence band it is appropriate to compare the spectrum with the SCDOS curve. A thorough theoretical analysis and full numerical simulation for the case when two-electron emissions originate from sp–sp-, sp–d-, or d–d-type states have been presented in a previous study[74]. The experimental results which are in line with a previous study[74] exhibit a significantly higher intensity in the sp–d region compared with the SCDOS. This reveals band-resolved configurations of electron pairs and the need to use a band-dependent formulation of electron correlation. The new experimental facility with improved energy resolution will also provide an additional approach to study the correlated electron emission dynamics. We have shown that the intrinsically fast Auger-type transitions allow to make statements about the timescale of the correlated electron dynamics, in particular the pair emission due to the neutralization of a He^{2+} ion. The two neutralization steps could be compared with a pump-probe experiment. The time delay was statistical in nature and cannot be adjusted experimentally. The use of a HHG source offers the control of the delay between say an infrared pump pulse and the VUV light. In this way the time-scale of correlated electron dynamics can be studied.

3. Conclusion

Starting from a general overview on the dominant mechanisms that lead to two time-correlated vacuum electrons upon the impact of a single photon or a single charged particle impact, we provided several typical examples on the measured spectra and how one can access the strength of the electron–electron interaction and separate the role of exchange. We also discussed Auger processes and how to possibly access the timescale of the emission process. In this regard not much has been done yet both experimentally and theoretically. So far the time resolution of our experiments has been way below the femto-to-attosecond

timescale of the involved electronic processes. Theoretically, all theories so far in this area were formulated in the standing flux scheme, leading to stationary theory. In recent years however there has been remarkable advance in producing femtosecond electron bunches but the coincidence electronic and the repetition rate of the bunches are still challenges. From a conceptional point of view one may state that the two-particle correlation is not simply a constant (such as U) but it has an internal structure, as shown by the two-particle energy and momentum spectra. While these observations are made at higher energies and are relevant to the particle–particle and hole–hole channel, it is conceivable that this general behavior is maintained at lower energies down to the particle–hole regime, where indeed it has been shown that in numerous cases higher orders in the electron–electron multiple scattering are needed, for example, to account for excitonic effects.

Conflict of Interest

The authors declare no conflict of interest.

[1] *Solid-State Photoemission and Related Methods Theory and Experiment* (Eds. W. Schattke, M. van Hove), Wiley-VCH, Weinheim, Germany **2003**.

[2] E. Weigold, I. E. McCarthy, *Electron Momentum Spectroscopy*, Kluwer Academic/Plenum Publishers, New York, London **1999**.

[3] P. Storer, R. S. Caprari, S. A. C. Clark, M. Vos, E. Weigold, *Rev. Sci. Instrum.* **1994**, *65*, 2214.

[4] I. E. McCarthy, E. Weigold, *Rep. Prog. Phys.* **1991**, *54*, 789.

[5] Y. Zheng, J. J. Neville, C. E. Brion, *Science* **1995**, *270*, 786.

[6] R. Camilloni, G. Stefani, R. Fantoni, A. Giardini-Guidoni, *J. Electron. Spectrosc. Relat. Phenom.* **1979**, *17*, 209.

[7] R. Camilloni, A. G. Guidoni, R. Tiribelli, G. Stefani, *Phys. Rev. Lett.* **1972**, *29*, 618.

[8] O. M. Artamonov, S. N. Samarin, J. Kirschner, *Appl. Phys. A* **1997**, *65*, 535.

[9] S. Samarin, R. Herrmann, H. Schwabe, O. Artamonov, *J. Electron. Spectrosc. Relat. Phenom.* **1998**, *96*, 61.

[10] A. Bellissimo, G. M. Pierantozzi, A. Ruocco, G. Stefani, O. Y. Ridzel, V. Astašauskas, W. S. M. Werner, M. Taborelli, *J. Electron Spectrosc. Relat. Phenom.* **2019**, 146883.

[11] S. Iacobucci, L. Marassi, R. Camilloni, S. Nannarone, G. Stefani, *Phys. Rev. B* **1995**, *51*, R10252.

[12] F. Da Pieve, D. Sébilleau, S. Di Matteo, R. Gunnella, R. Gotter, A. Ruocco, G. Stefani, C. R. Natoli, *Phys. Rev. B* **2008**, *78*, 035122.

[13] J. Berakdar, M. P. Das, *Phys. Rev. A* **1997**, *56*, 1403.

[14] R. Herrmann, S. Samarin, H. Schwabe, J. Kirschner, *Phys. Rev. Lett.* **1998**, *81*, 2148.

[15] M. Hattass, T. Jahnke, S. Schössler, A. Czasch, M. Schöffler, L. Ph, H. Schmidt, B. Ulrich, O. Jagutzki, F. O. Schumann, C. Winkler, J. Kirschner, R. Dörner, H. Schmidt-Böcking, *Phys. Rev. B* **2008**, *77*, 165432.

[16] J. L. Powell, B. Crasemann, *Quantum Mechanics*, Dover Publications, New York, USA **2015**.

[17] J. Berakdar, *Phys. Rev. B* **1998**, *58*, 9808.

[18] Y. Pavlyukh, M. Schüler, J. Berakdar, *Phys. Rev. B* **2015**, *91*, 155116.

[19] M. Schüler, Y. Pavlyukh, P. Bolognesi, L. Avaldi, J. Berakdar, *Sci. Rep.* **2016**, *6*, 24396.

[20] A. Ruocco, W. S. M. Werner, M. I. Trioni, S. Iacobucci, G. Stefani, *Phys. Rev. B* **2017**, *95*, 155408.

[21] W. S. M. Werner, A. Ruocco, F. Offi, S. Iacobucci, W. Smekal, H. Winter, G. Stefani, *Phys. Rev. B* **2008**, *78*, 233403.

[22] a) J. Berakdar, S.N. Samarin, R. Herrmann, J. Kirschner, *Phys. Rev. Lett.* **1998**, *81*, 3535; b) S. Samarin, J. Berakdar, O.M. Artamonov, H. Schwabe, J. Kirschner, *Surf. Sci.* **2000**, *470*, 141.

[23] N. Fominykh, J. Berakdar, J. Henk, P. Bruno, *Phys. Rev. Lett.* **2002**, *89*, 086402.

[24] a) H. Gollisch, G. Meinert, X. Yi, R. Feder, *Solid State Commun.* **1997**, *102*, 317; b) J. Berakdar, H. Gollisch, R. Feder, *Solid State Commun.* **1999**, *112*, 587.

[25] F. O. Schumann, J. Kirschner, J. Berakdar, *Phys. Rev. Lett.* **2005**, *95*, 117601.

[26] K. A. Kouzakov, J. Berakdar, *Phys. Rev. Lett.* **2003**, *91*, 257007.

[27] a) A. Lahmam-Bennani, I. Taouil, A. Duguet, M. Lecas, L. Avaldi, J. Berakdar, *Phys. Rev. A* **1999**, *59*, 3548; b) J. Berakdar, A. Lahmam-Bennani, C. Dal Cappello, *Phys Rep.* **2003**, *374*, 91.

[28] A. Morozov, J. Berakdar, S. N. Samarin, F. U. Hillebrecht, J. Kirschner, *Phys. Rev. B* **2002**, *65*, 104425.

[29] S. Samarin, O. M. Artamonov, A. D. Sergeant, J. Kirschner, A. Morozov, J. F. Williams, *Phys. Rev. B* **2004**, *70*, 073403.

[30] S. N. Samarin, J. F. Williams, O. M. Artamonov, J. Henk, R. Feder, *Surf. Sci.* **2010**, *604*, 1833.

[31] a) R. Feder, F. Giebels, H. Gollisch, *Phys. Rev. B* **2015**, *92*, 075420; b) D. Vasilyev, F.O. Schumann, F. Giebels, H. Gollisch, J. Kirschner, R. Feder, *Phys. Rev. B* **2017**, *95*, 115134; c) K.A. Kouzakov, L. Chotorlishvili, J. Wätzel, J. Berakdar, A. Ernst, *Phys. Rev. A* **2019**, *100*, 022311.

[32] S. Samarin, J. Berakdar, A. Suvorova, O. M. Artamonov, D. K. Waterhouse, J. Kirschner, J. F. Williams, *Surf. Sci.* **2004**, *548*, 187.

[33] a) H. Ibach, D. Bruchmann, R. Vollmer, M. Etzkorn, P.S. Anil Kumar, J. Kirschner, *Rev. Sci. Instrum.* **2003**, *74*, 4089; b) K. Zakeri, Y. Zhang, T. H. Chuang, J. Kirschner, *Phys. Rev. Lett.* **2012**, *108*, 197205.

[34] M. Streun, G. Baum, W. Blask, J. Berakdar, *Phys. Rev. A* **1999**, *59*, R4109.

[35] G. A. van Riessen, F. O. Schumann, M. Birke, C. Winkler, J. Kirschner, *J. Phys.: Condens. Matter* **2008**, *20*, 442001.

[36] F. O. Schumann, R. S. Dhaka, G. A. van Riessen, Z. Wei, J. Kirschner, *Phys. Rev. B* **2011**, *84*, 125106.

[37] I. S. Brandt, Z. Wei, F. O. Schumann, J. Kirschner, *Phys. Rev. Lett.* **2014**, *113*, 107601.

[38] I. S. Brandt, Z. Wei, F. O. Schumann, J. Kirschner, *Phys. Rev. B* **2015**, *92*, 155106.

[39] C. Tusche, J. Kirschner, *Rev. Sci. Instrum.* **2014**, *85*, 063305.

[40] C. Tusche, *Phys. Rev. Lett.* **2015**, *115*, 027602.

[41] C. H. Li, C. Tusche, F. O. Schumann, J. Kirschner, *Phys. Rev. Lett.* **2017**, *118*, 136402.

[42] C.-T. Chiang, M. Huth, A. Trützschler, M. Kiel, F. O. Schumann, J. Kirschner, W. Widdra, *New J. Phys.* **2015**, *17*, 013035.

[43] M. Huth, C.-T. Chiang, A. Trützschler, F. O. Schumann, J. Kirschner, W. Widdra, *Appl. Phys. Lett.* **2014**, *104*, 061602.

[44] A. Trützschler, M. Huth, C.-T. Chiang, R. Kamrla, F. O. Schumann, J. Kirschner, W. Widdra, *Phys. Rev. Lett.* **2017**, *118*, 136401.

[45] B. D. Napitu, J. Berakdar, *Phys. Rev. B* **2010**, *81*, 195108.

[46] F. O. Schumann, Y. Aliaev, I. Kostanovskiy, G. Di Filippo, Z. Wei, J. Kirschner, *Phys. Rev. B* **2016**, *93*, 235128.

[47] F. O. Schumann, L. Behnke, C. H. Li, J. Kirschner, *J. Phys.: Condens. Matter* **2013**, *25*, 094002.

[48] F. O. Schumann, C. Winkler, J. Kirschner, *Phys. Rev. Lett.* **2007**, *98*, 257604.

[49] F. O. Schumann, C. Winkler, J. Kirschner, F. Giebels, H. Gollisch, R. Feder, *Phys. Rev. Lett.* **2010**, *104*, 087602.

[50] F. Giebels, H. Gollisch, R. Feder, F. O. Schumann, C. Winkler, J. Kirschner, *Phys. Rev. B* **2011**, *84*, 165421.

[51] J. Berakdar, *Nucl. Instrum. Methods Phys. Res. B* **2000**, *171*, 204.

[52] F. Giebels, H. Gollisch, R. Feder, *J. Phys.: Condens. Matter* **2009**, *21*, 355002.

[53] I. S. Brandt, Z. Wei, J. Kirschner, F. O. Schumann, *Phys. Rev. B* **2019**, *100*, 075139.

[54] F. O. Schumann, L. Behnke, C. H. Li, J. Kirschner, Y. Pavlyukh, J. Berakdar, *Phys. Rev. B* **2012**, *86*, 035131.

[55] Z. Wei, F. O. Schumann, C. H. Li, L. Behnke, G. Di Filippo, G. Stefani, J. Kirschner, *Phys. Rev. Lett.* **2014**, *113*, 267603.

[56] I. Kostanovskiy, F. O. Schumann, Y. Aliaev, Z. Wei, J. Kirschner, *J. Phys.: Condens. Matter* **2016**, *28*, 015601.

[57] S. P. Kowalczyk, L. Ley, R. L. Martin, F. R. McFeely, D. A. Shirley, *Faraday Discuss. Chem. Soc.* **1975**, *60*, 7.

[58] G. Wendin, M. Ohno, S. Lundqvist, *Solid State Commun.* **1976**, *19*, 165.

[59] G. Wendin, *Breakdown of the One Electron Pictures in Photoelectron Spectra*, Springer Verlag, Berlin, Heidelberg, New York **1981**.

[60] U. Fano, *Phys. Rev.* **1961**, *124*, 1866.

[61] J. E. Muller, O. Jepsen, O. K. Andersen, J. W. Wilkins, *Phys. Rev. Lett.* **1978**, *40*, 720.

[62] J. Feist, S. Nagele, R. Pazourek, E. Persson, B. I. Schneider, L. A. Collins, J. Burgdörfer, *Phys. Rev. Lett.* **2009**, *103*, 063002.

[63] J. Feist, R. Pazourek, S. Nagele, E. Persson, B. I. Schneider, L. A. Collins, J. Burgdörfer, *J. Phys. B: At., Mol. Opt. Phys.* **2009**, *42*, 134014.

[64] M. L. E. Oliphant, *Proc. R. Soc. A* **1930**, *127*, 373.

[65] H. D. Hagstrum, *Phys. Rev.* **1954**, *96*, 336.

[66] H. D. Hagstrum, G. E. Becker, *Phys. Rev. Lett.* **1971**, *26*, 1104.

[67] P. A. Zeijlmans van Emmichoven, P. A. A. F. Wouters, A. Niehaus, *Surf. Sci.* **1988**, *195*, 115.

[68] N. Lorente, R. Monreal, *Surf. Sci.* **1994**, *303*, 253.

[69] S. Wethekam, A. Mertens, H. Winter, *Phys. Rev. Lett.* **2003**, *90*, 037602.

[70] H. D. Hagstrum, G. E. Becker, *Phys. Rev. B* **1973**, *8*, 107.

[71] J. Viefhaus, S. Cvejanovicacute, B. Langer, T. Lischke, G. Prümper, D. Rolles, A. V. Golovin, A. N. Grum-Grzhimailo, N. M. Kabachnik, U. Becker, *Phys. Rev. Lett.* **2004**, *92*, 083001.

[72] L. Folkerts, J. Das, S. W. Bergsma, R. Morgenstern, *Phys. Lett. A* **1992**, *163*, 73.

[73] E. De Filippo, G. Lanzanò, H. Rothard, C. Volant, *Phys. Rev. Lett.* **2008**, *100*, 233202.

[74] N. Fominykh, J. Henk, J. Berakdar, P. Bruno, *Surf. Sci.* **2002**, *507*, 229.